MOLECULAR IMAGING AND BIOLOGY

Mol Imaging Biol (2016) 18:109–116
DOI: 10.1007/s11307-015-0868-y

Published Online: 9 June 2015

RESEARCH ARTICLE

Automatic Cardiac Self-Gating of Small-Animal PET Data

Joaquin L. Herraiz,[1,2] Elena Herranz,[3,4] Jacobo Cal-González,[5] Juan J. Vaquero,[6,7] Manuel Desco,[6,7,8] Lorena Cussó,[6,7,8] Jose M. Udias[2]

[1]*Madrid-MIT M+Vision Consortium, Massachusetts Institute of Technology, Cambridge, MA, USA*
[2]*Grupo de Física Nuclear, Universidad Complutense de Madrid, CEI Moncloa, Madrid, Spain*
[3]*A.A.Martinos Center for Biomedical Imaging, Massachusetts General Hospital, Charlestown, MA, USA*
[4]*Harvard Medical School, Boston, MA, USA*
[5]*Center for Medical Physics and Biomedical Engineering, Medical University of Vienna, Vienna, Austria*
[6]*Departamento de Ingenieria Biomedica e Ingeniería Aeroespacial, Universidad Carlos III de Madrid, Leganés, Spain*
[7]*Instituto de Investigación Sanitaria Gregorio Marañón, Madrid, Spain*
[8]*Centro de Investigación Biomédica en Red de Salud Mental (CIBERSAM), Barcelona, Spain*

Abstract

Purpose: The cardiac gating signal (CGS) in positron emission tomography (PET) studies is usually obtained from an electrocardiography (ECG) monitor. In this work, we propose a method to obtain the CGS in small-animal PET using the acquired list-mode data without using any hardware or end-user input.

Procedures: The CGS was obtained from the number of coincidences over time acquired in the lines-of-response connected with the cardiac region. This region is identified in the image as its value changes with frequencies in the range of 3 to 12 Hz. The procedure was tested in a study with 29 Wistar rats and 6 mice injected with 2-deoxy-2-[^{18}F]fluoro-D-glucose, which underwent a 45-min single-bed list-mode PET scan of the heart syncronized with an ECG. The estimated signals and the reconstructed images using eight-gated frames were compared with the ones obtained using the ECG signal from the monitor.

Results: The differences of the PET-based CGS with respect to the ECG relative to the duration of the heartbeats were 5.6 % in rats and 11.0 % in mice. The reconstructed gated images obtained from the proposed method do not differ qualitatively with respect to the ones obtained with the ECG. The quantitative analysis of both set of images were performed measuring the volume of the left ventricle (LV) of the rats in the end-of-systole and end-of-diastole phase. The differences found in these parameters between both methods were below 12.1 % in the ESV and 9.3 % in the EDV with a 95 % confidence interval, which are comparable to the accuracy (7 %) of the method used for segmenting the LV.

Conclusion: The proposed method is able to provide a valid and accurate CGS in small-animal PET list-mode data.

Key words: List-mode, PET, Small animal, Cardiac gating, Self-gating

Correspondence to: Joaquin Herraiz; *e-mail:* herraiz@mit.edu

Introduction

Cardiac positron emission tomography (PET) is a well-established technique routinely used in clinical and preclinical applications for non-invasive imaging and quantification of myocardial metabolism, perfusion, and receptor density [1]. Cardiac research increasingly relies on small animals to monitor gene expression *in vivo* and physiologic parameters [2]. In these studies, accurate measurements of the end-diastolic (EDV) and end-systolic (ESV) volume of the left ventricle (LV), and the cardiac ejection fraction (EF) are important to define normal values and to monitor the effect of different therapeutic strategies in disease models [3–6].

LV volume and EF can be measured by means of cardiac-gated (PET) using 2-deoxy-2-[^{18}F]fluoro-D-glucose ([^{18}F]FDG) [2], in which the PET raw data are divided into time subsets (gates) corresponding to the different phases of the heartbeat. This results in a set of reconstructed images ("gated images") of these phases, each one with much reduced motion.

Cardiac gating of PET acquisitions is usually achieved using an electrocardiography (ECG) monitor. Its signal is acquired simultaneously with the PET data and based on it, a cardiac gating signal (CGS) that reflects the starting time of each heartbeat is stored within the list-mode data [3].

Nevertheless, the use of additional equipment such as the ECG has some disadvantages, as it requires extra time/effort during setup, and the reliability of the experiment depends on the ability and skills in configuring this setup. In some preclinical settings, this additional equipment may not be available, or it may not work properly during an acquisition, and furthermore, it is usually rather cumbersome to use in small animals. Moreover, the use of these systems requires the integration of software, hardware, and user input, which could be problematic [7]. Recently, it has been shown that the CGS derived from an ECG may have a significant amount of errors, such as missing heartbeats, which may worsen the quality of the gated images [7]. Therefore, it would be desirable to be able to reconstruct an adequate CGS directly from the measured PET data without any additional equipment or input from the user.

Automatic and self-contained cardiac and respiratory motion detection (that is, without resourcing to additional equipment to the PET imaging system) has already been proposed for human scanners [8]. Indeed, estimation of the respiratory and cardiac motions have been obtained from either the variation of the number of counts with time in the whole acquisition [9], in a few axial slices [10], in some voxels of the reconstructed images [11], or as a function of counts in large sinogram bins [12] have been obtained.

However, to our knowledge, these kind of automatic retrospective cardiac gating methods have not been successfully applied to small-animal PET acquisitions. The determination of the cardiac motion in rodents is more challenging because their cardiac frequency (300–800 bpm) is significantly higher than the human one. Indeed, our attempts on our small-animal acquisitions to employ methods based on the variation of counts in the whole acquisition or on particular slices did not provide enough signal-to-noise ratio (SNR) to isolate the cardiac motion signal.

In this work, we propose to improve this SNR by the precise determination of the left ventricle as the region of interest (ROI) in the field-of-view (FOV) with the largest variation in the number of emissions per second at a rate compatible with the expected heartbeat frequencies. Using only emissions coming from this small ROI, we were able to obtain enough SNR from the acquired PET data so as to generate a precise CGS.

We evaluated its performance with [^{18}F]FDG-PET acquisitions from rodents using a preclinical scanner. We compared the retrospective CGS and the final reconstructed gated images with the ones obtained using the standard external ECG.

Materials and Methods

Data Acquisition

Data were acquired with a high-resolution small-animal ARGUS PET-CT scanner (Sedecal, Spain) [13]. This tomograph has a transaxial FOV of 68 mm and an axial one of 48 mm, and it is able to obtain images with sub-millimetric resolution using iterative reconstruction [14].

The data acquired with this scanner are organized by default as LOR-histogram files [15]. Nevertheless, it may also acquire and store data for dynamic and gated acquisitions in list-mode files. These files contain the LOR number that defines a crystal detector pair for each measured coincidence, plus timing information every 33 ms. External information from respiratory and cardiac measurements can be included in the list files in steps of 0.655 ms.

In this work, we used acquisitions of 29 Wistar rats (14 controls and 15 with myocardial infarction after permanent occlusion of the left anterior descending artery [6]), with 300 g and 420 heartbeats per minute (bpm) on average, and 6 mice, with 26 g and 540 bpm on average. The inclusion of rats with up to 40 % of infarcted myocardium allowed verifying the method in challenging but common conditions is preclinical cardiac PET imaging. All animal procedures were approved by the Animal Experimentation Ethics Committee of Hospital General Universitario Gregorio Marañón, Madrid, Spain and were performed according to EU directive 2010/63/EU and national regulations (RD 53/2013). PET scans were performed 60 min after intravenous injection of [^{18}F]FDG (35 MBq in rats and 20 MBq in mice). ECG-gated cardiac PET data were acquired for 45 min.

ECG signal was recorded by an external system (Omicrom VISION—PET, RGB, Spain) specifically developed to record and analyze the ECG signal from the rodents and to generate a binary gate signal (i.e., the CGS) at the beginning of every cardiac cycle. This external CGS was available in all the list-mode data analyzed in this work.

The CGS is used to divide the acquisition into a user-defined number of gated frames. At this step, the standard scanner's software rejects coincidences that belong to heartbeats 10 % larger or shorter than the average, as obtained from the CGS. This avoids potential artifacts in the reconstructed images caused by missing beats or errors in the processing of the ECG signal [7] and typically affects to 5 % of the data.

Automatic Location of the Cardiac ROI

In order to automatically find the location of the LV, we analyzed the initial 2 min of the list-mode data divided into sets of 16.375 ms. The LORs in each set were back-projected in 3-D mode, without any filtering, into a low spatial resolution volume of 55×55×21 voxels (corresponding to a voxel size of 1.3×1.3×2.4 mm^3). We used a home-made code in Fortran based on the Siddon ray-tracing algorithm [16] for this purpose. The size of the voxels and the temporal bin size chosen ensure enough spatial and time resolution, while accumulating enough number of counts in each voxel. One of the key insights of this work is that this simple (unfiltered) back-projection is enough to obtain the information of the variation of counts with time in each voxel, without requiring any sinogram binning and/or filtering.

The variation of counts over time in each individual voxel was analyzed in the frequency domain. Voxels in the left ventricle have a clear peak in the frequency spectrum, corresponding to cardiac motion (Fig. 1a, in red), while this peak is not visible in voxels far outside the cardiac region (Fig. 1a, in blue). The position and width of this peak is similar in the spectrum of the CGS obtained from the external ECG (Fig. 1a, in black).

We defined the cardiac motion signal-to-noise ratio (CM-SNR) for each voxel in the back-projected volume as

$$\text{CM-SNR} = \left(\frac{\text{Max-bg}}{\text{bg}}\right)^2 \quad (1)$$

Max represents the maximum amplitude of the power spectrum within the frequency range explored of 3 Hz – 12 Hz and bg is the background level of that power spectrum (Fig. 1a, in red). For a voxel located in the left ventricle, the CM-SNR has a significant large value, while for all the other voxels is basically noise with zero mean (Fig. 2a).

As the CM-SNR in mice is typically very small, an additional step is required to get the correct identification of the cardiac region. The value of Max in mice is obtained after averaging neighboring voxels in the complex frequency domain. Voxels that are moving in phase, get reinforced with this average, while voxels with values not correlated with their neighbors show smaller values after this average.

In this way, the CM-SNR in the cardiac region increases significantly with respect to other areas, and the procedure can be applied to both mice and rat acquisitions. Once the CM-SNR image is obtained (Fig. 2a), we select the ROI with the cardiac motion. The cardiac ROI (Fig. 2b, c) is heuristically defined as the set of voxels with CM-SNR values greater than 2/3 of the maximum CM-SNR in the whole image.

We quantified the detectability of the cardiac region in the CM-SNR image according to the Rose model of statistical detection [17] as

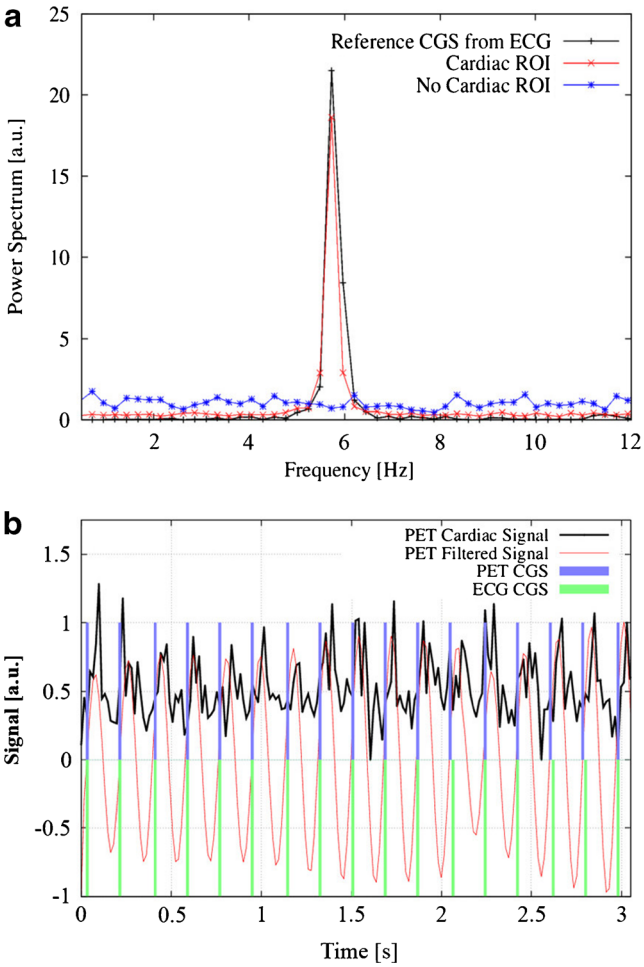

Fig. 1 **a** Frequency spectrum of the coincidence rate from the cardiac ROI (*red*) and from outside of the cardiac ROI (*blue*). The peak in the cardiac spectrum agrees with the one in the gating signal from the ECG (*black*). **b** Ratio of counts in the cardiac ROI respect to the counts outside of it, using time frames of 0.1675 ms (*black*), its filtered version (*red*), and the CGS derived from it (*blue*), together with the CGS from the ECG (*green*, with negative values for better display).

$$\text{Detectability} = \frac{C-B}{3\sigma_B} \quad (2)$$

where C is the average value in the cardiac ROI, and B and σ_B are the mean and standard deviation of the background in the CM-SNR image evaluated at least 10 mm away from the cardiac ROI.

Extraction of the Cardiac Gating Signal from the LORs Connected to the Cardiac ROI

Once the cardiac ROI is identified, we obtain a weight for each LOR that indicates their degree of connection with this ROI. We obtain these weights by a forward projection code similar to the one used for the backward projection. All events in the list-mode data are then weighted with these values, and the resulting total number of weighted counts in 16.375 ms time bins constitute our raw

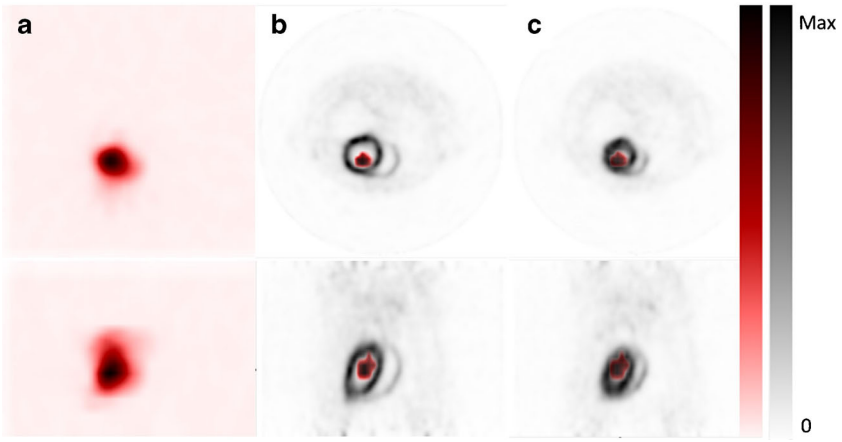

Fig. 2 The hottest region in the CM-SNR image (**a**) defines the cardiac ROI (**b**, **c**) used for obtaining the CGS. As expected, this ROI corresponds with the left ventricle region as shown in the gated images reconstructed from the same acquisition. Using eight cardiac-gated frames based on the ECG signal, diastole (**b**) corresponds to gate 7, and systole (**c**) to gate 3.

cardiac signal. The rest of the recorded counts are considered a background signal. In a typical rat study, the amount of LORs connected to the selected ROI is usually in the order of 20 % (~6 million LORs), and the number of counts per bin of 16.375 ms is about 200. In mice acquisitions, due to the smaller size of the cardiac region, this number decreases to about 5 % (~1.5 million LORs), with 50 counts per bin. To reduce the possible errors in the data transmission and storage in the list-mode file, which could create spurious fluctuations of counts with time, the raw cardiac signal is divided by the background signal to generate the cardiac signal (Fig. 1b).

This cardiac signal is then band-pass filtered with a second-order Butterworth filter centered at the frequency of the maximum of the frequency spectrum. This step reduces the noise caused by the low number of coincidences detected in each heart cycle and the Poisson statistical nature of the process. The filtering process was performed using a sliding time window of 512 time points of 16.375 ms, to take into account the variations of the heartbeat frequency and possible cardiac arrhythmia during the PET acquisition.

The filtered data in the time domain (Fig. 1b in red) represent the variation of emissions from the cardiac ROI in each heartbeat. The CGS is obtained from this signal evaluating for each cardiac cycle the time point in which the signal changes its sign from negative to positive. We used this reference as the starting point of each cardiac cycle as it correlates well with the CGS provided by the ECG (Fig. 1b in green). It is important to note that the origin of the CGS is somewhat arbitrary, and that the external ECG-derived CGS signal may have some constant delay in the process of injecting it into the PET list mode data stream. Therefore, if there were not an exact correspondence of these CGSs, we could have obtained a globally shifted derived gated signal, and a simple global phase shift would have rendered the external ECG-CGS and the data-driven CGS more comparable.

In order to validate the method, the resulting CGS t_i^{est} of each acquisition was compared to the one t_i^{ref} obtained with the external ECG, which can be considered the gold standard. For each heartbeat, we obtained $\Delta t_i=(t_i^{\text{est}}-t_i^{\text{ref}})/T_i^{\text{heartbeat}}$ the relative time difference between both signals, with respect to the duration T_i of each heartbeat. We did not consider in this analysis those heartbeats that, according to the CGS, have a duration larger or shorter than 10 % of the average. Since they are likely to have a wrong CGS, they are actually discarded by the scanner's software. For each acquisition with N valid heartbeats, we computed the root mean square of the relative errors:

$$\text{RMSRE} = \sqrt{\sum_i^N (\Delta t_i)^2/N} \tag{3}$$

We obtained the mean and standard deviation of these results for the total number of rats and mice.

We created a version of the list-mode data files, in which we exchanged the original ECG-CGS by our CGS. We preserved the format and size of the original files, so that they could be processed following the normal reconstruction procedure for this scanner.

Data Gating, Image Reconstruction, and Analysis

List-mode data were divided into eight independent-gated frames using the CGS derived from our method and using the CGS from the ECG. The data of each gated frame were stored in LOR-histogram files and reconstructed separately with the fully 3D iterative reconstruction code FIRST (fast iterative reconstruction software for PET tomography) [14] using 1 iteration of 40 subsets. FIRST is based on a realistic model of radiation emission and detection, which obtains images with sub-millimetric resolution with low noise levels. The number of voxels in these gated reconstructed images was set to 175×175×61, with a size of 0.3875×0.3875×0.775 mm.

We evaluated the impact of using the proposed self-gating method on a cardiac parameter of interest such as the EDV, ESV, and EF of the LV in the 29 rats, as compared to the use of standard ECG-based gating (Fig. 6a). For this purpose, we used a semi-automatic cardiac segmentation tool for nuclear medicine images available within the Segment [18]. This tool calculates the volume of the LV in each phase of the heartbeat in the reconstructed images. The software requires as input from the user a selection of the axial planes containing the cardiac region (typically around 11 slices of 0.775 mm thickness), as well as the location of a point

inside the heart. Small variations of these inputs generated deviations in the derived EF of 7 % on average. The method comparison was performed with the Bland-Altman plot [19] for the ESV and EDV.

Results

The results from the method outlined in this work to locate automatically the cardiac region can be seen in Fig. 2. On the left, the CM-SNR image clearly shows the cardiac region. The center and right images shows the cardiac ROI, segmented by thresholding the CM-SNR image, fused with reconstructed images using eight cardiac frames gated based on the ECG signal. The center image corresponds to the diastole (gate 7/8), and the right image corresponds to the systole (gate 3/8). It can be seen that the cardiac ROI corresponds to the center of the left ventricle of the rat.

The impact of the amount of data used on the ability of identifying the cardiac region was quantified with the detectability parameter defined in (2) in the same rat acquisition. Using only 500 time bins of 33 ms, the detectability was 1.1, which indicates that the cardiac ROI could only be detected with difficulty. With 1000 time bins of 33 ms, the resulting detectability was 6.4, high enough to identify the heart without difficulty. With 4000 time bins (132 s of acquisition), we obtained the CM-SNR shown in Fig. 2a, the detectability reached a value of 24.3.

In the rest of this work, we used the initial 120 s for the identification of the cardiac region. The processing time for this identification is less than 1 min in a single core of a common CPU (3.0 GHz Intel(R) Xeon(R) 64 bit processor).

We compared the results obtained with the proposed PET-based CGS, with the ones using the standard ECG-based CGS in different domains. We performed the comparison in the derived signals (Figs. 3 and 4) in rats and mice, and the reconstructed gated images (Fig. 5), and some cardiac parameters (Fig. 6) in rats.

Figure 3 shows the quantitative results of the differences in the CGS obtained with both methods. For all rats considered in this study (N=29), the mean of the RMSRE (between the PET-CGS and the ECG-CGS), in each acquisition, was 5.6±2.0 %. For the mice (n=6), the mean of the RMSRE was 11.0±2.8 % (Fig. 3). No statistical difference was found between control and infarcted rats (two sample t test, P>0.05). These results indicate that the differences in the CGS are smaller than the duration of one frame in a typical study with eight cardiac frames.

As a further comparison of the CGS obtained with the method outlined in this work and the external ECG signal, in Fig. 4, the instant heartbeat rate is displayed along the whole acquisition for one typical control rat. The vertical line at 120 s indicates the moment in which enough data have been acquired and analyzed to start using this method for monitoring the heart rate based only on the PET data.

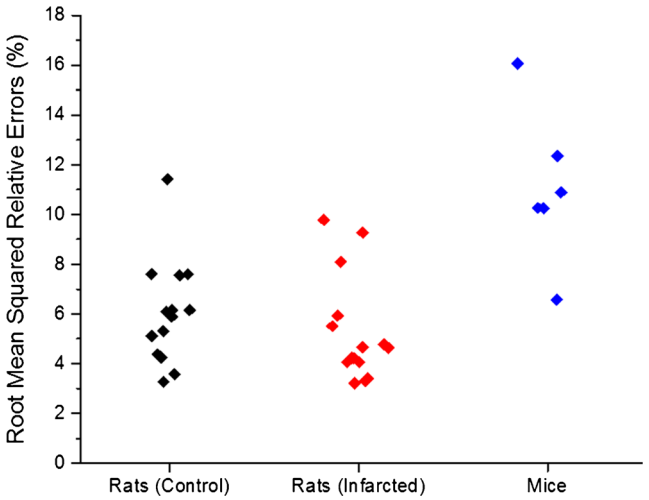

Fig. 3 Root mean squared (RMSRE) of the differences in the estimated CGS respect to the ECG-based CGS, relative to the duration of each heartbeat for the control rats, the infarcted rats, and the mice.

Transverse and sagittal views of images reconstructed with the 3D-OSEM iterative reconstruction software FIRST, gated using eight frames with the self-gating method, are shown in Fig. 5. It can be seen that the motion of the heart is adequately frozen. Further, count profiles along reconstructed images, gated with the external ECG and with the proposed method, are compared in Fig. 5d.

The profiles along the heart of the gated images obtained from both methods are essentially indistinguishable, and in both cases, the thickness of the myocardium is clearly reduced compared to the non-gated case, which is blurred by the cardiac motion.

Figure 6a shows the EF, LV-EDV, and LV-ESV of the 29 rats of the study (control and infarcted) calculated with the images gated with the proposed method using only the PET data compared with the ones gated with the ECG (standard method). As it is shown in the Bland-Altman plot in Fig. 6b, c, the bias was 1.1 % for the ESV and −0.7 % for the EDV, and the 95 % confidence interval limits, at 1.96

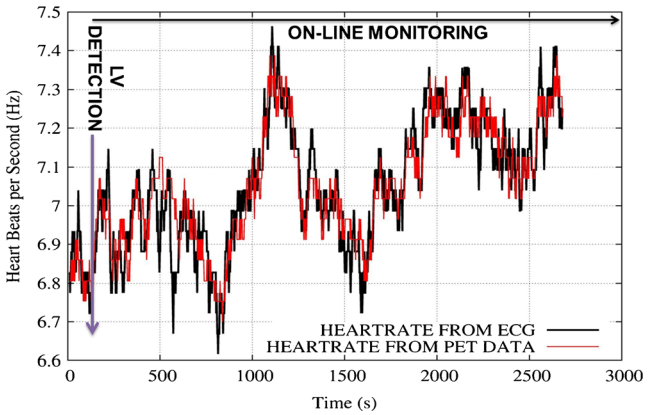

Fig. 4 Demonstration of the heart rate monitoring capabilities of the proposed method in a control rat.

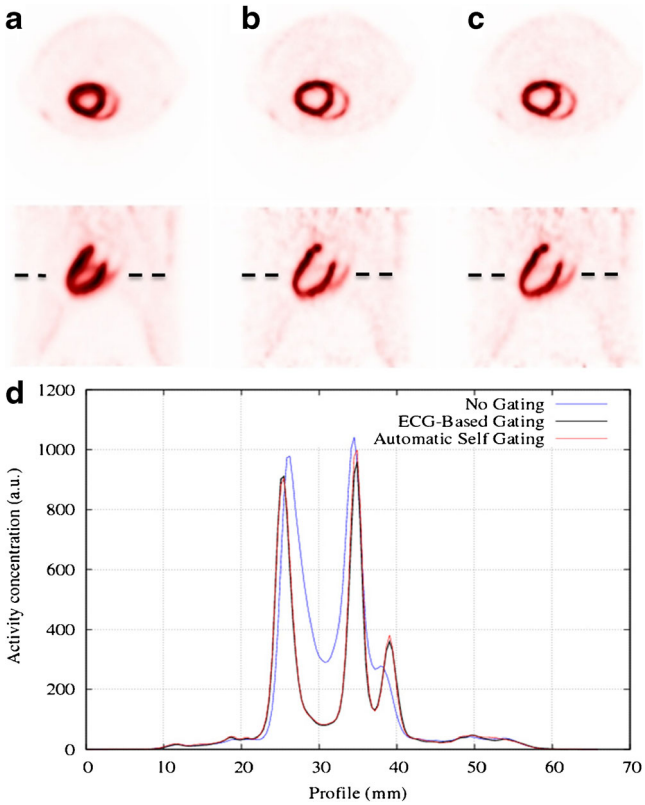

Fig. 5 **a** Images of a control rat using no gating, **b** eight frames gated based on the ECG signal, and **c** based on the proposed method. In both cases, transverse (*above*) and sagittal (*below*) views are shown. **d** Profiles along the heart in these three images are shown.

standard deviations (SD), corresponds to relative deviations of 12.1 % in the ESV and 9.3 % in the EDV. Therefore, the SD of the differences is smaller than the accuracy of 7 % that we estimated for the segmentation procedure with the Segment tool.

Discussion

The goal of this paper was to study the feasibility of obtaining the CGS directly from the PET data in small-animal acquisitions. This possibility could significantly simplify the acquisition setup in many preclinical cardiac PET studies, in which the use of cardiac gates is required to study the EF, or to obtain high-resolution "motion-free" images [4].

This CGS required a very precise selection of the data containing the cardiac signal in order to obtain a sufficient SNR. The procedure has been validated against a reference cardiac signal obtained from an external ECG monitor. It has been shown to be a robust procedure as we found no failures (i.e., impossibility of recovering the CGS) in any of the cases analyzed, even when serious conditions of several hearts (with up to 40 % of infarcted myocardium) were involved. It is remarkable that we were able to obtain the CGS even in mouse studies with the heartbeat about 540 bpm, the total amount of activity in the myocardium is low, and the cardiac region is small.

The quantitative analysis of the results showed that the mean squared error of the differences in the time marks between both signals (i.e., the CGS) was about 6 % in rats and 11 % in mice relative to the heartbeat period, which can be considered acceptable in most studies as it may be smaller than other sources of uncertainty. A recent work [7] has shown that the ECG-based CGS in small animals is not perfect, and some errors may be expected. In our case, about 5 % of the heartbeats are missed by the ECG. In fact, even though we considered the ECG signal as our reference, we cannot consider it as a perfect ground truth.

We also used this analysis to evaluate the propagation of errors in the gating signal to the results of the EF. This provides a good way to determine how precisely the CGS should be derived to get reasonably accurate results (i.e., within the uncertainties of the methods for image analysis) in this kind of preclinical studies. Finally, we evaluated the propagation of errors in the determination of the CGS into the results of the derived EF. We obtained that errors of the order of 5 % in the CGS were propagated into similar errors (of the order of 7 %) in the ESV and EDV, which is actually similar to the accuracy of the segmentation procedure. These results indicate that small deviations in the CGS (a few percent) are not very significant for the final results obtained in these studies.

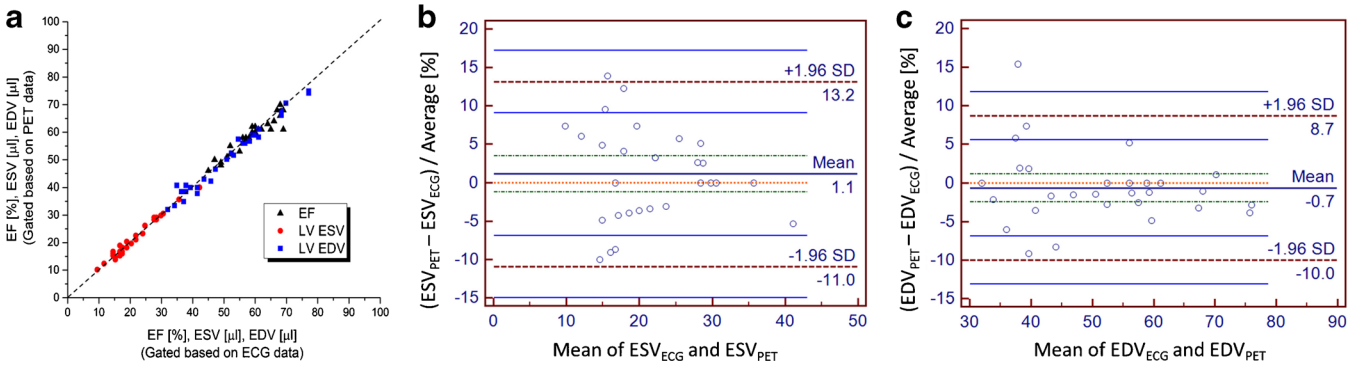

Fig. 6 **a** Scatter diagram of the EDV, ESV, and EF of the LV of the 29 rats obtained with images gated using the ECG and gated with the method proposed. Bland-Altman plot of **b** the ESV and **c** the EDV.

The ESV, EDV, and EF in rats was obtained from the reconstructed gated images with an semi-automatic segmentation tool available in Segment, which is freely available for academic purposes. The advantage of using a tool like this is that it provides a straightforward way to compare the gating images obtained with each method, reducing a possible variability in the result caused by manual segmentation. We only compared the EF in rats, as a reliable measurement in the small heart of the mice with Segment was much harder. In any case, from our results with the rats, we may assume that deviations in the EF would be similar to the deviations obtained in the CGS.

We found no significant differences in the results when using rats with a cardiac infarct. with respect to control ones (Fig. 3), which demonstrates the robustness of the method.

The proposed method is so effective in the location of the heart that could provide a way of detecting possible animal motions during the acquisition. This could be achieved by monitoring the location of the heart at every single moment in the acquisition retrospectively, or by using the real-time monitoring of the heart rate as shown in Fig. 3. Sudden small displacement of the thorax would lead to a sudden drop in the heartbeat rate derived from the emissions coming from the selected cardiac ROI. This information could be used, for instance, to divide the acquisition in separated motionless time frames, or to incorporate it into a reconstruction software which could handle motion correction. This procedure could be also extended to human acquisitions in a quite straightforward way.

As already mentioned, a short acquisition, typically 2-min long is enough to identify accurately the cardiac region, and the processing time to obtain it is less than 1 min. Therefore, the time required to obtain the cardiac signal from the PET data is very modest and almost real-time CGS can be obtained. Of course, if needed, this could be further speeded-up using multi-core execution or implementing it in modern and powerful GPUs [20].

In this work, we did not explore the possibility of performing the analysis of the whole acquisition in the image domain, with a similar approach as the one we employ to locate the cardiac ROI. This option would be more computational demanding, but it could simplify the method, as it would remove the step forward projection of the cardiac ROI.

The method may be applied to any other PET scanner, as long as their sensitivity is high enough to collect a sufficient number of counts in each heartbeat and the available list-mode data has enough time resolution.

The possibility of extending this work to dynamic acquisitions is being studied. The early frames of a dynamic cardiac imaging study, right after the injection, are very challenging for a method like this, as almost no activity in the myocardium is yet present. Nevertheless, as soon as there is some uptake in the heart, the method should work as well as in the static acquisition.

Conclusions

This work proposes an automatic cardiac-gating procedure for small-animal [^{18}F]-FDG-PET acquisitions. The results shown here demonstrate that it is possible to obtain the gating signal from a list-mode PET acquisition of rats and mice, by studying the variation with time of the counts in the region most affected by the cardiac motion. To our knowledge, this is the first time this has been achieved in rodents. The method can be also employed to improve results on self-contained cardiac and respiratory gating in human PET acquisitions.

The deviations in the obtained CGS, EDV, ESV, and in the EF measured on the resulting gated images with respect to the ECG-based reference are not significant, taking into account the typical uncertainties of the quantitative measurements in preclinical PET.

In this work, we also propose a procedure to automatically identify the heart in image space by means of fast back-projecting a small fraction of the acquired data. This localization procedure can be used for automatic cardiac segmentation and heart beat monitoring.

Acknowledgments. This work was supported in part by Consejería de Educación, Juventud y Deporte de la Comunidad de Madrid (Spain) through the Madrid-MIT M+Visión Consortium, Comunidad de Madrid (S2013/MIT-3024 TOPUS-CM), UCM (Grupos UCM, 910059), CPAN (Consolider-Ingenio 2010, CSPD-2007-00042), RIC-RETIC network, Spanish MINECO (RD12/0042/0057), Ministerio de Ciencia e Innovación, Spanish Government (ENTEPRASE grant, PSE-300000-2009-5 and TEC2007-64731/TCM), and European Regional funds.

Conflict of Interest. All authors declare that they have no competing interest.

References

1. Di Carli MF, Lipton MJ (2007) Cardiac PET and PET/CT Imaging. Springer Science and Business Media
2. Wu JC, Inubushi M, Sundaresan G et al (2002) Positron emission tomography imaging of cardiac reporter gene expression in living rats. Circulation 106:180–183
3. Yang Y, Rending S, Siegel S et al (2005) Cardiac PET imaging in mice with simultaneous cardiac and respiratory gating. Phys Med Biol 50:2979–2989
4. Croteau E, Bénard F, Cadorette J et al (2003) Quantitative gated PET for the assessment of the left ventricular function in small animals. J Nucl Med 44:1655–1661
5. Cussó L, Hernandez-Porras I, Montesinos P et al (2013) Phenotyping K-RasV141 knock-in mouse by cardiac-MRI: a pilot study. World Mol Imag Cong (WMIC): Program Book. pp. 79
6. Cussó L, Santa Marta C, Benito M et al (2009) Multimodal assessment of myocardial infarction in rats: comparison of late gadolinium enhanced MRI and PET. Abstract Eur Soc Mol Imag (ESMI). pp. 104
7. Böning G, Todica A, Vai A et al (2013) Erroneous cardiac ECG-gated PET list-mode trigger events can be retrospectively identified and replaced by an offline reprocessing approach: first results in rodents. Phys Med Biol 58:7937–7959
8. Dineley J (2010) Fully automated gating: a new era for PET?, http://medicalphysicsweb.org/cws/article/research/44273
9. He J, O'Keefe GJ, Gong SJ et al (2008) A novel method for respiratory motion gated with geometric sensitivity of the scanner in 3D PET. IEEE Trans Nucl Sci 55:2557–2565
10. Büther F, Dawood M, Wübbeling F et al (2009) List mode-driven cardiac and respiratory gating in PET. J Nucl Med 50:674–681

11. Kesner AL, Bundschuh RA, Detorieet NC et al (2009) Respiratory gated PET derived in a fully automated manner from Raw PET data. IEEE Trans Nucl Sci 56:677–687
12. Kesner AL, Kuntner C (2010) A New fast and fully automated software based algorithm for extracting respiratory signal from raw PET data and its comparison to other methods. Med Phys 37:5550–5559
13. Wang Y, Seidel J, Tsui BMW et al (2006) Performance evaluation of the GE healthcare eXplore VISTA dual-ring small-animal PET scanner. J Nucl Med 47:1891–1900
14. Herraiz JL, España S, Vaquero JJ et al (2006) FIRST: fast iterative reconstruction software for (PET) tomography. Phys Med Biol 51:4547–4565
15. Kadrmas DJ (2004) LOR-OSEM: statistical PET reconstruction from raw line-of-response histograms. Phys Med Biol 49:4731–4744
16. Siddon RL (1985) Fast calculation of the exact radiological path for a three-dimensional CT array. Med Phys 12:252–255
17. Mancosu P, Sghedoni R, Bettinardi V et al (2009) 4D-PET data sorting into different number of phases: a NEMA IQ phantom study. J Appl Clin Med Phys 10:220–231
18. Heiberg E, Sjogren J, Ugander M et al (2010) Design and validation of segment—freely available software for cardiovascular image analysis. BMC Med Imaging 10:1 (http://segment.heiberg.se)
19. Bland JM, Altman DG (1986) Statistical methods for assessing agreement between two methods of clinical measurement. Lancet 1(8476):307–310
20. Herraiz JL, España S, Cal-González J et al (2011) Fully 3D GPU PET reconstruction. Nucl Inst Methods Phys Res A 648:S169–S171